

# Effects of injection beam parameters and foil scattering for CSNS/RCS\*

HUANG Ming-Yang(黄明阳)<sup>1)</sup> WANG Sheng(王生) QIU Jing(邱静)

WANG Na(王娜) XU Shou-Yan(许守彦)

Institute of High Energy Physics, Chinese Academy of Sciences, Beijing 100049, China

**Abstract:** The China Spallation Neutron Source (CSNS) uses  $H^-$  stripping and phase space painting method to fill a large ring acceptance with a small emittance linac beam. The dependence of the painting beam on the injection beam parameters was studied for the Rapid Cycling Synchrotron (RCS). The simulation study was done for injection with different momentum spreads, different rms emittances of the injection beam, and different matching conditions. Then, the beam loss, 99% and rms emittances were obtained, and the optimized injection beam parameters were given. The interaction between  $H^-$  beam and stripping foil was studied, and the effect of foil scattering was simulated. The stripping efficiency was calculated and the suitable thickness of stripping foil was obtained. In addition, the energy deposition on the foil and the beam loss due to the foil scattering were also studied.

**Key words:** CSNS, RCS, injection parameter, foil scattering

**PACS:** 29.25.Dz, 29.27.Ac, 41.85.Ar **DOI:** 10.1088/1674-1137/37/6/067001

## 1 Introduction

The China Spallation Neutron Source (CSNS) is a high power proton accelerator-based facility [1]. The accelerator consists of a 1.6 GeV the Rapid Cycling Synchrotron (RCS) and an 80 MeV  $H^-$  linac which is upgradable to 250 MeV. The RCS accumulates  $1.56 \times 10^{13}$  protons in two intense bunches and operates at a 25 Hz repetition rate with a design beam power of 100 kW, and is capable of upgrading to 500 kW. It has a four-fold lattice with four long straight sections for the injection, extraction, Radio Frequency (RF) and beam collimation.

For high intensity proton accelerators, injection via  $H^-$  stripping is a practical method. The design of the RCS injection system is to inject  $H^-$  beam into the RCS with high precision and high transport efficiency. In order to control the strong space charge effects, which are the main causes of the beam loss in CSNS/RCS, the phase space painting method is used for injecting a small emittance beam from the linac into the large ring acceptance [2]. By using the ORBIT code [3], the multi-turn phase space painting injection process with space charge effects for CSNS/RCS is studied in detail.

When the  $H^-$  beam traverses the stripping foil, most of the particles  $H^-$  are converted to  $H^+$ , and the others are converted to  $H^0$  or unchanged. The interaction between  $H^-$  beam and stripping foil can induce additional

beam loss. By using the FLUKA code [4], the effect of foil scattering is simulated, and the stripping efficiency is calculated. The energy deposition on the foil and the beam loss due to the foil scattering are also studied.

## 2 Dependence of the painting beam on the injection beam parameters

For CSNS, a combination of the  $H^-$  stripping and the phase space painting method is used to accumulate a high intensity beam in the RCS. Fig. 1 shows the layout of the RCS injection system [2] and Table 1 shows the main injection parameters [5]. For the beam injection, three kinds of orbit-bumps are prepared [2]: a horizontal bump (four dipole magnets; BH1–BH4) for painting in  $x-x'$  plane; a vertical bump (four dipole magnets; BV1–BV4) for painting in  $y-y'$  plane; a horizontal bump (four dipole magnets; BC1–BC4) in the middle for an additional closed-orbit shift of 57 mm.

The beam loss can be divided into two kinds: the longitudinal beam loss, occurs when the particles are outside the RF bucket or beyond the momentum acceptance of the machine; the transverse beam loss, occurs when the particles exceed the collimator's acceptance. For CSNS, although it has a large ring acceptance, the nonlinear part of the space charge force will lead to non-uniformity of the beam distribution, and beam loss will probably

Received 23 August 2012

\* Supported by National Natural Science Foundation of China (11205185, 11175020, 11175193)

1) E-mail: huangmy@ihep.ac.cn

©2013 Chinese Physical Society and the Institute of High Energy Physics of the Chinese Academy of Sciences and the Institute of Modern Physics of the Chinese Academy of Sciences and IOP Publishing Ltd

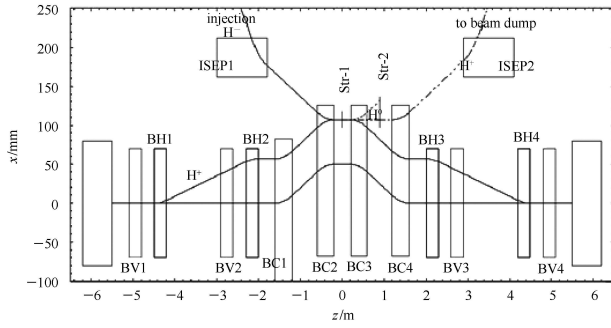


Fig. 1. Layout of the RCS injection system.

Table 1. Main injection parameters of CSNS/RCS.

parameters/units	values
circumference/m	227.92
injection energy/GeV	0.08
extraction energy/GeV	1.6
injection beam power/kW	5
extraction beam power/kW	100
nominal betatron tunes	4.86/4.78
RF frequency/MHz	1.0241–2.3723
RF voltage/kV	165
harmonic number	2
repetition rate/Hz	25
number of particles per pulse	$1.56 \times 10^{13}$
momentum acceptance (%)	1
painting scheme	anti-correlated
chopping rate (%)	50
turn number of injection	200

happen. In order to reduce the beam loss, painting into the large acceptance with good uniformity is usually required. One parameter indicating the influence of the space charge effects is the tune shift. In the case of uniform distribution, the tune shift due to the space charge effects can be expressed by:

$$\Delta\nu = -\frac{r_p N_t}{2\pi\beta^2\gamma^3\epsilon B_f}, \quad (1)$$

where  $r_p = 1.53 \times 10^{-18}$  m is the classical proton radius,  $N$  is the accumulated particles,  $\epsilon$  is the un-normalized emittance,  $B_f$  is the longitudinal bunching factor,  $\beta$  and  $\gamma$  are the Lorentz factors. It can be found from Eq. (1) that, the tune shift will change with the varying beam parameters, such as the emittance and bunching factor.

Some work had been done for the injection parameters optimization [6, 7]. In this section, the effects of the momentum spread, the rms emittance of injection beam, and the mismatch injection twiss parameters are discussed in detail. In the following simulation, the chopping rate is 50%, the patterns of the RF voltage and synchrotron phase are given in Fig. 2, and the space charge effects are considered. The turn number of the injection painting process is 200, and the first 2000 turns in the acceleration process are considered in the simulation.

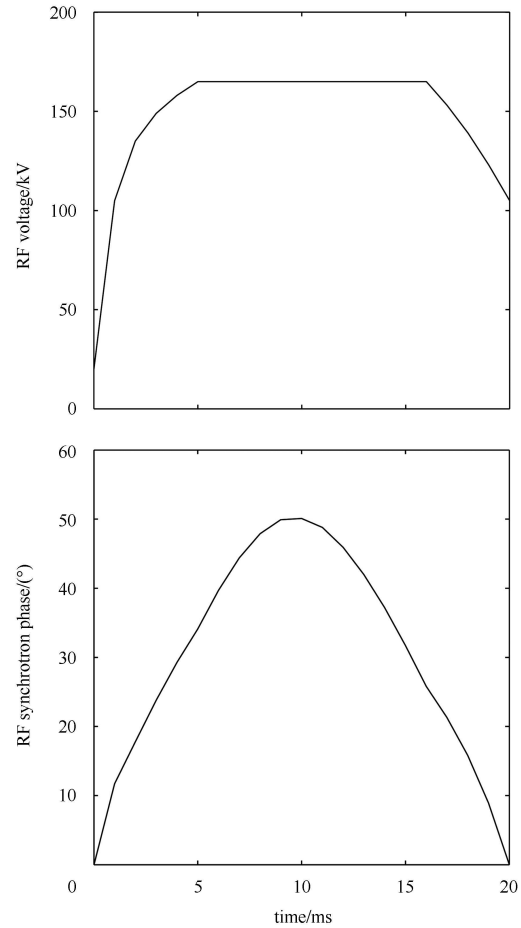


Fig. 2. The patterns of the RF voltage and synchrotron phase over the acceleration period.

## 2.1 Momentum spread

In order to study the effects of the momentum spread, the injection processes with the momentum spread between 0.01% and 0.5% were simulated. Fig. 3 shows the beam loss, 99% and rms emittances as functions of the momentum spread and Fig. 4 shows the rms emittance evolution for different momentum spreads. It can be found from Fig. 3 that the beam loss decreases firstly and then increases with the increasing momentum spread. While the momentum spread is smaller than 0.1%, the beam loss is smaller than 1%, the 99% and rms emittances are constrained in reasonable ranges.

It can be found from Fig. 4 that there is transverse coupling which depends on the momentum spread. When the momentum spread is below 0.1%, the coupling becomes stronger with the increasing momentum spread. However, when the momentum spread is above 0.1%, the coupling becomes weaker with the increasing momentum spread. Therefore, the momentum spread of 0.1% is a optimal value for injection. This simulation results are consistent with the operation experience in J-PARC [8].

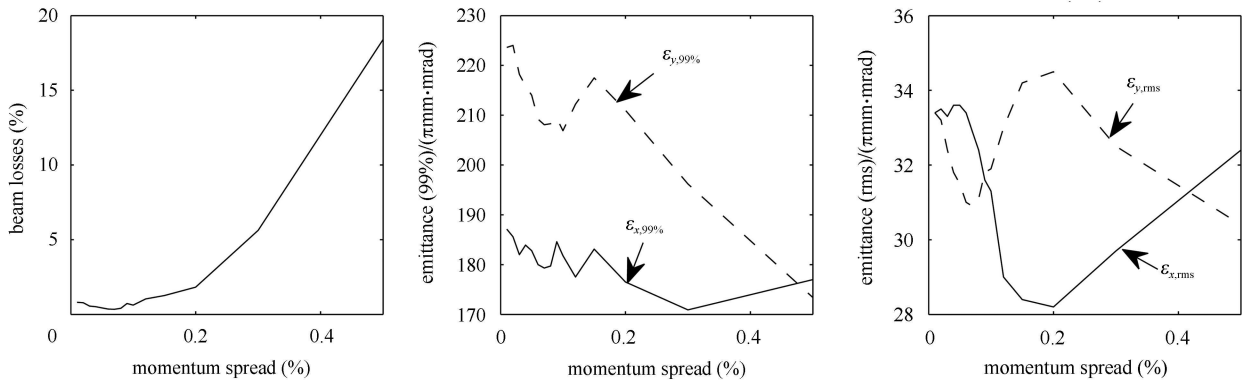


Fig. 3. Beam loss, 99% and rms emittances as functions of the momentum spread.

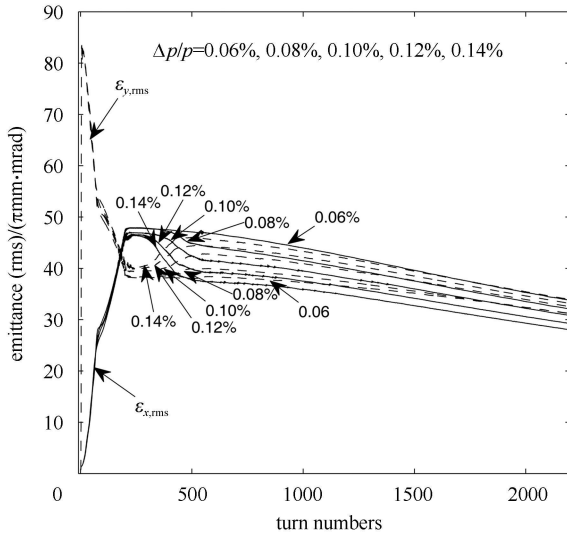


Fig. 4. The rms emittance evolution for different momentum spreads.

## 2.2 rms emittance of injection beam

In order to study the effects of the rms emittance of injection beam, the injection processes with the rms emittance between  $0.1 \pi\text{mm}\cdot\text{mrad}$  and  $5.0 \pi\text{mm}\cdot\text{mrad}$

were simulated. Fig. 5 shows the beam loss, 99% and rms emittances as functions of the rms emittance of injection beam. It can be found that the beam loss, 99% and rms emittances all increase with the increasing rms emittance of injection beam. In addition, while the rms emittance of injection beam is smaller than  $1.0 \pi\text{mm}\cdot\text{mrad}$ , the beam loss is smaller than 1%, the 99% and rms emittances are constrained in reasonable ranges.

## 2.3 Mismatch injection twiss parameters

For the RCS design, it has been a primary concern to match the emittance of the linac beam to the RCS acceptance at the injection point. A mismatched injection could result in large beam loss and an undesirable transverse emittance growth. The first condition for the injection beam matching is obtained by choosing the parameters [9]:

$$\frac{\alpha_l}{\beta_l} = \frac{\alpha_r}{\beta_r}, \quad (2)$$

where  $\alpha_l$  and  $\beta_l$  are the twiss parameters for the linac, and  $\alpha_r$  and  $\beta_r$  are that for the RCS. For CSNS,  $\alpha_r$  nearly equals 0. In order to study the effects of the injection twiss parameters mismatch, for a fixed  $\beta_l$ , different  $\alpha_l$  were discussed.

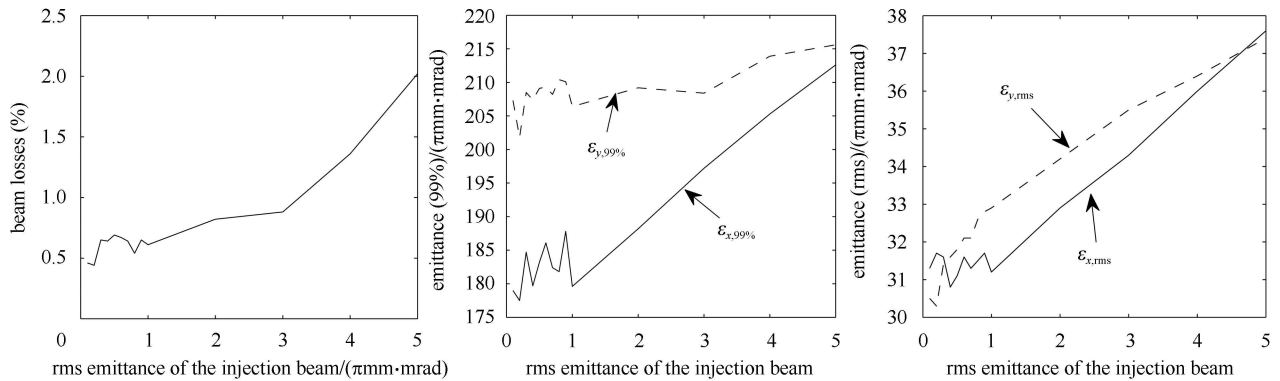
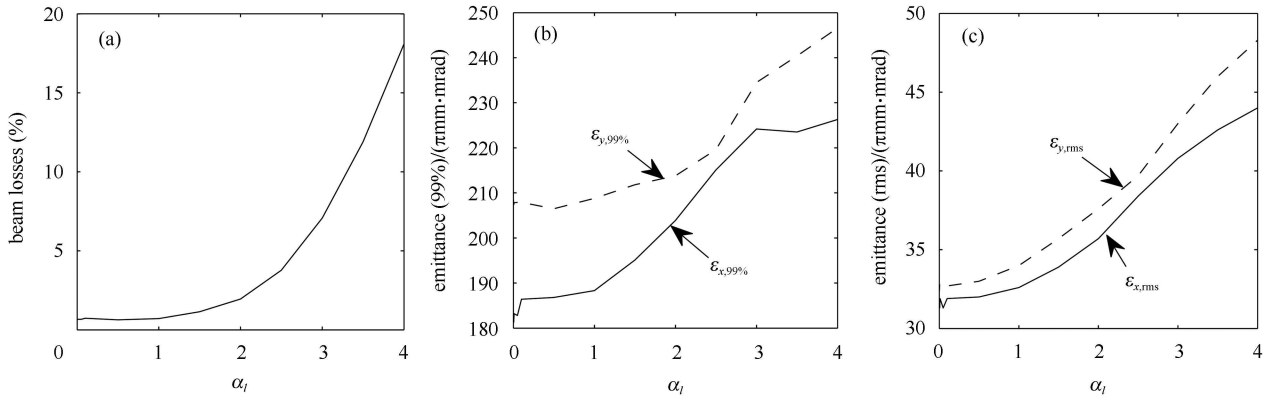


Fig. 5. Beam loss, 99% and rms emittances as functions of the rms emittance of injection beam.


 Fig. 6. Beam loss, 99% and rms emittances as functions of  $\alpha_l$ .

The injection processes with  $(\alpha_{lx}, \alpha_{ly})$  between  $(0.0, 0.0)$  and  $(5.0, 5.0)$  were simulated. Fig. 6 shows the beam loss, 99% and rms emittances as functions of  $\alpha_l$ . It can be found that the beam loss, 99% and rms emittances all increase with the increasing  $\alpha_l$ . While  $(\alpha_{lx}, \alpha_{ly})$  is smaller than  $(1.0, 1.0)$ , the beam loss is smaller than 1%, the 99% and rms emittances are constrained in reasonable ranges, i.e., the effects of the mismatched injection are very small. However, while  $(\alpha_{lx}, \alpha_{ly})$  is larger than  $(1.0, 1.0)$ , the beam loss, 99% and rms emittances are much larger than that of the matching case.

### 3 Foil scattering effects

In the RCS injection system, there are two carbon stripping foils: a primary stripping foil and a secondary stripping foil. In this part, the interaction between  $H^-$  beam and the stripping foil is discussed [10–12], and the stripping efficiency is calculated. The energy deposition on the foil and the beam loss due to the foil scattering are also studied.

#### 3.1 Foil stripping

When the  $H^-$  beam traverses the carbon stripping foil [13], there are six charge exchange processes: three are electron loss reactions and the other three are electron pickup reactions. However, for energies above 100 keV, the cross sections for electron pickup are very small and can be neglected. Therefore, the remaining particles after foil stripping are  $H^-$ ,  $H^0$  and  $H^+$ , as shown in Fig. 7. The stripping efficiency of  $H^+$  is given by [14]

$$f_{H^+} = 1 - \frac{1}{\sigma_{-1,0} + \sigma_{-1,1} - \sigma_{0,1}} [\sigma_{-1,0} e^{-\sigma_{0,1}x} - (\sigma_{0,1} - \sigma_{-1,1}) e^{-(\sigma_{-1,0} + \sigma_{-1,1})x}], \quad (3)$$

where  $\sigma_{-1,0}$ ,  $\sigma_{0,1}$ ,  $\sigma_{-1,1}$  are the cross-sections of the reactions  $H^- \rightarrow H^0 + e^-$ ,  $H^0 \rightarrow H^+ + e^-$ , and  $H^- \rightarrow H^+ + e^- + e^-$ ,

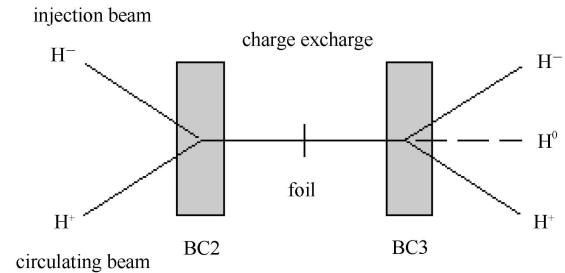
respectively. In addition,  $x = N_o \tau / A$ , where  $N_o$  is Avogadro's constant,  $A$  is the atomic number of carbon foil, and  $\tau$  is the area density. The percentage that the  $H^-$  beam traverses the carbon foil without stripping is given by [14]

$$f_{H^-} = e^{-\sigma_{-1,0}x}. \quad (4)$$

Therefore, the yielding rate of  $H^0$  can be expressed as

$$f_{H^0} = 1 - f_{H^+} - f_{H^-}. \quad (5)$$

There are some studies [14, 15] about the cross-sections  $\sigma_{-1,0}$ ,  $\sigma_{0,1}$ ,  $\sigma_{-1,1}$ , and it shows that these cross-sections depend on the beam energy. Table 2 shows a summary of the cross-sections at 80 MeV and 250 MeV.


 Fig. 7. The production of  $H^-$ ,  $H^0$ ,  $H^+$  by foil stripping.

Using Eqs. (3)–(5) and the cross-sections given in Table 2, the relations between  $f_{H^+}$ ,  $f_{H^0}$ ,  $f_{H^-}$  and the foil thickness can be obtained. Fig. 8 shows that  $f_{H^+}$ ,  $f_{H^0}$ ,  $f_{H^-}$  vary with the foil thickness. It can be found that, with the increasing foil thickness,  $f_{H^+}$  increases,  $f_{H^-}$  decreases, and  $f_{H^0}$  has a maximum value. For a given foil thickness, the stripping efficiency for 80 MeV injection is larger than that for 250 MeV injection. In order to make the stripping efficiency greater than 99.7%, the foil thickness needs to be larger than  $100 \mu\text{g}/\text{cm}^2$  for 80 MeV injection and  $240 \mu\text{g}/\text{cm}^2$  for 250 MeV injection.

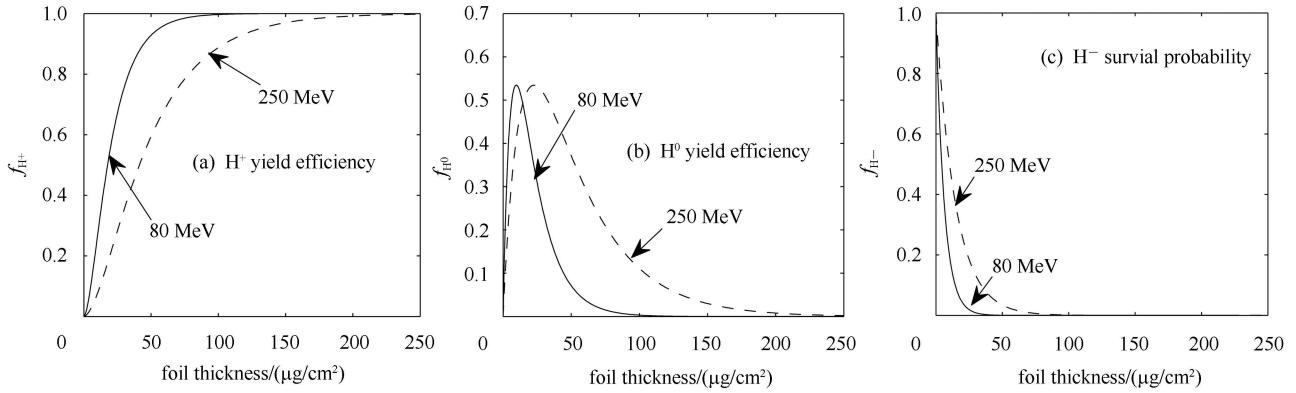

 Fig. 8.  $H^-$ ,  $H^0$ ,  $H^+$  yielding rates as functions of the foil thickness.

 Table 2. Cross-sections of  $H^-$  incident on carbon foil (unit  $10^{-18}\text{cm}^2$ ).

	80 MeV	250 MeV
$\sigma_{-1,0}$	3.17	1.35
$\sigma_{0,1}$	1.24	0.53
$\sigma_{-1,1}$	0.056	0.024

### 3.2 Energy deposition on the foil

When the  $H^+$  beam traverses the stripping foil, there is energy deposition on the foil. The energy deposition depends on the beam energy and the foil thickness [12]. In this part, the relations between the energy deposition and the foil thickness for different injection energy are studied.

The foil scattering processes were simulated by using the FLUKA code. Fig. 9 shows the energy deposition on the foil as a function of the foil thickness. For both 80 MeV injection and 250 MeV injection, it was

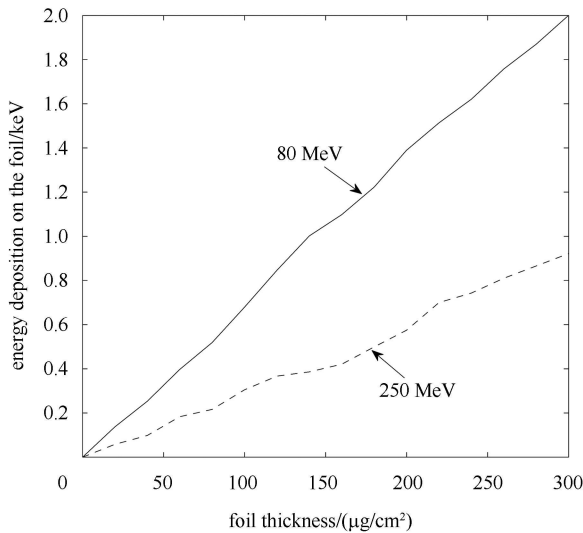


Fig. 9. The energy deposition as a function of the foil thickness.

found that the energy deposition increases with the increasing foil thickness. In addition, the relations between the energy deposition and the foil thickness are nearly linear. Furthermore, the energy deposition on the foil is 0.68 keV for each 80 MeV  $H^+$  particle ( $100 \mu\text{g}/\text{cm}^2$ ) and 0.74 keV for each 250 MeV  $H^+$  particle ( $240 \mu\text{g}/\text{cm}^2$ ).

### 3.3 Beam loss

During the injection process, while the proton beam traverses the stripping foil, the foil scattering will lead to additional beam loss. For J-PARC, the stripping foil scattering had been studied and it was found that the foil scattering was the main cause of the beam loss in the injection region [16]. Therefore, the beam loss due to the foil scattering for CSNS/RCS also needs to be studied in detail.

For a given proton flux and target element, the production event number of scattering particle can be given by

$$N(i) = N_T \cdot I \cdot \int dE \cdot \sigma(i) \cdot \phi_i(E), \quad (6)$$

where  $i$  stands for different kinds of scattering particles,  $N_T$  is the target number,  $I$  is the interaction probability,  $\sigma(i)$  is the crossing section, and  $\phi(i)$  is the given proton flux. However, in order to study the beam loss due to the foil scattering, the multi-turn particle tracking and particle scattering need to be studied together. By using the FLUKA and ORBIT codes, the injection process and foil scattering can be simulated. Table 3 shows the beam parameters for 80 MeV injection and 250 MeV injection.

By using the ORBIT code, the average traversal number and the beam distribution after injection can be obtained. Calculating those particles of the beam distribution which are in the range of stripping foil, the twiss parameters and 99% emittance for those particles can be obtained, as shown in Table 4. With these beam parameters, the beam that hitting on the stripping foil can

be simulated. Then, the foil scattering process can be simulated by using the FLUKA code and the beam loss in a single turn can be obtained. By using the average traversal number, the beam loss in the multi-turn injection can be calculated. Table 5 shows a summary of the beam loss due to the foil scattering. It can be found that

Table 3. Beam parameters for 80 MeV injection and 250 MeV injection.

injection	80 MeV	250 MeV
injection beam power/kW	5	80
average injection current/ $\mu\text{A}$	62.5	312.5
turn number of injection	200	403
foil thickness/ $(\mu\text{g}/\text{cm}^2)$	100	240

Table 4. Beam parameters of the proton distribution that hitting on the stripping foil.

injection	80 MeV	250 MeV
$(\alpha_x, \alpha_y)$	(0.003, 0.044)	(0.001, 0.016)
$(\beta_x, \beta_y)/\text{m}$	(1.833, 4.458)	(1.877, 5.222)
$(\gamma_x, \gamma_y)/\text{m}^{-1}$	(0.546, 0.225)	(0.533, 0.192)
$(\varepsilon_{x,99\%}, \varepsilon_{y,99\%})/(\pi\cdot\text{mm}\cdot\text{mrad})$	(92, 247)	(90, 282)

Table 5. Beam loss due to the stripping foil scattering.

injection	80 MeV	250 MeV
average traversal number	5	10
particle loss ratio in single turn	0.0012%	0.00058%
total beam losses/W	0.3	4.6

the beam loss is about 0.3 W for 80 MeV injection and 4.6 W for 250 MeV injection.

## 4 Conclusions

The dependence of the painting beam on the injection beam parameters for CSNS/RCS were studied, and the simulation was done for different momentum spreads, different rms emittance of the injection beam, and different matching conditions. It was found that, in order to make the beam loss smaller than 1% and constrain the 99% and rms emittances in reasonable ranges, the momentum spread needs to be smaller than 0.1%, the rms emittances of the injection beam need to be smaller than  $1.0 \pi\text{mm}\cdot\text{mrad}$ , and  $(\alpha_{lx}, \alpha_{ly})$  need to be smaller than (1.0, 1.0). In addition, the momentum spread of 0.1% is an optimal value for injection.

The interaction between  $\text{H}^-$  beam and stripping foil was studied. In order to make the stripping efficiency achieve 99.7%, the foil thickness needs to be larger than  $100 \mu\text{g}/\text{cm}^2$  for 80 MeV injection and  $240 \mu\text{g}/\text{cm}^2$  for 250 MeV injection. The energy aggradation while the  $\text{H}^+$  beam traverses the stripping foil was studied. It was found that the relations between the energy aggradation and the foil thickness were nearly linear for both 80 MeV injection and 250 MeV injection. Finally, The beam loss due to the foil scattering was studied. It was found that the beam loss was about 0.3 W for 80 MeV injection and about 4.6 W for 250 MeV injection.

*The authors would like to thank their CSNS colleagues for discussions and consultations.*

## References

- 1 WANG S, FANG S X, FU S N et al. Chin. Phys. C, 2009, **33**: 1–3
- 2 TANG J Y, QIU J, WANG S et al. Chin. Phys. C, 2006, **30**: 1184–1189
- 3 Gabambos J, Holmes J, Olsen D. ORBIT User's Manual V1.0. SNS-ORNL-AP Tech. Note 11, 1999
- 4 Ferrari A, Fasso A, Ranft J et al. Fluka: Multi-Particle Transport Code. CERN-2005-010, 2008
- 5 CSNS Project Team. China Spallation Neutron Source Feasibility Reaearch Report. Institute of High Energy Physics and Institute of Physics, Chinese Academy of Sciences, 2009 (in Chinese)
- 6 QIU J, TANG J Y, WANG S et al. Chin. Phys. C, 2007, **31**: 942–946
- 7 WEI T, WANG S, QIU J et al. Chin. Phys. C, 2010, **34**: 218–223
- 8 WEI G H. Beam Injection and Fast Extraction Tuning of the J-PARC MR, and Some Study on the J-PARC Linac. IHEP Report, January 2012
- 9 Beebe-Wang J, Prior C R. Injection Mismatch for the SNS Accumulator Ring. BNL/SNS TECHNICAL NOTE, NO. 086, June 1, 2000
- 10 Mohagheghi A H, Bryant H C, Harris P G et al. Phys. Rev. A, 1991, **43**: 1345–1365
- 11 Saha P K, Hatakeyama S, Yamamoto K et al. Phys. Rev. ST Accel. Beams, 2011, **14**: 072801
- 12 Drozhdin A I, Rakhno I L, Striganov S I et al. Phys. Rev. ST Accel. Beams, 2012, **15**: 011002
- 13 Gulley M S, Keating P B, Bryant H C et al. Phys. Rev. A, 1996, **53**: 3201–3210
- 14 Webber R C, Hojvat C. IEEE Trans. Nucl. Sci. NS-26, 1979. 4012–4014
- 15 CHOU W, Kostin M, TANG Z. Nucl. Instrum. Methods Phys. Res. A, 2008, **590**: 1–12
- 16 Akasaka N, Koiso H, Oide K et al. Operation Software for Commissioning of KEKB Linac Programmed with SAD. Proceedings of APAC, 1998. 495–497